Chemical Transformations in Ultrathin Chalcogenide Nanowires

Geon Dae Moon,[†] Sungwook Ko,[†] Younan Xia,[†,‡] and Unyong Jeong[†,*]

[†]Department of Materials Science and Engineering, Yonsei University, 134 Shinchon-dong, Seoul, Korea, and [‡]Department Biomedical Engineering, Washington University, St. Louis, Missouri 63130

ABSTRACT We have studied the chemical transformations in ultrathin chalcogenide nanowires with an aim to understand the parameters that control the morphology and crystal structure of the product. Ultrathin Te nanowires were transformed into Ag_2Te nanowires with preservation of the single crystallinity. The Ag_2Te nanowires were then converted into CdTe, ZnTe, and PbTe using cation-exchange reactions, and the CdTe nanowires were further transformed into $PtTe_2$ nanotubes. On the basis of the solubility products of the ionic solids, the crystal structures of the involved solids, the reaction kinetics, and the reaction conditions for transformations, we were able to reach the following conclusions: (i) The solubility products of ionic solids can be used as a rough criterion to predict if the transformation is thermodynamically favorable or not. (ii) The morphological preservation of reactant nanowires is more sensitive to the change in length rather than the total volume in addition to the lattice matching between the reactant and product nanowires. (iii) The crystal structure resulting from a transformation should be determined by the free energy of formation and the stability of the products. (iv) The transformation involving small volume change or topotactic lattice matching is considered homogeneous along the entire length of the nanowires, preserving both the single crystallinity and the morphology of the reactant nanowires.

KEYWORDS: chemical transformation · cation exchange · chalcogenide · nanowire · nanotube

Recently, chemical transformation of nanostructured materials has gained growing interest. The ability to transform existing materials enables us to greatly diversify the compositions of nanostructured materials.[1−4] It facilitates the synthesis of novel materials consisting of multiple components which may not be directly obtainable *via* a conventional synthesis. Furthermore, it might generate unprecedented shapes and unexpected crystal structures due to the mechanical stress accumulated during the transformation.[5−8] Among various chemical transformations, ion-exchange reactions have been extensively studied in the general areas of catalyst and thin film technology.[9,10] A number of cations such as Ag^+, Sb^{3+}, Bi^{3+}, and Cu^+ have been used to replace the Cd^{2+} ions in thin films of CdSe and CdS.[11−14] In principle, the ion-exchange strategy can be applied to all types of ionic semiconductors.

For the transformation of semiconductors, most studies have focused on the cation exchange of chalcogenides, whose crystal structures are determined by the frameworks of the chalcogen anions (S^{2-}, Se^{2-}, Te^{2-}). The metal cations are relatively mobile in the anionic framework, making it possible to replace the cations under moderate reaction conditions. Alivisatos and co-workers demonstrated that the cation-exchange reaction between Ag_2Se and CdSe nanocrystals was completely reversible by adjusting the reaction conditions.[15] Xia and co-workers showed that such transformation could be realized in mesoscale colloids.[16] Most recently, Son and co-workers started to investigate the effects of ion solvation and volume change on the morphology of resultant nanocrystals in the reactions of CdE → Pd_xE_y or Pt_xE_y (E = S, Se, Te).[17] They found that stronger solvation of Cd^{2+} lowered the activation energy for the transformation and facilitated the exchange between Cd^{2+} cations and Pd^{2+} or Pt^{2+} cations. They also found that a severe volume reduction could result in hollow nanocrystals, while a volume increase could break the structure into smaller pieces. It should be pointed out that this chemical transformation is different from the Kirkendall effect caused by the difference in diffusion flux between two chemical species. The formation of voids in the chemical transformation can be attributed to the release of the mechanical stress typically accumulated during a transformation reaction. Son and co-workers also suggested that the transformation mechanism may be dependent on the crystal structure of the reactant CdE nanocrystals.[17] However, the conditions for successful

*Address correspondence to ujeong@yonsei.ac.kr.

Received for review December 19, 2009 and accepted March 15, 2010.

Published online March 25, 2010.
10.1021/nn9018575

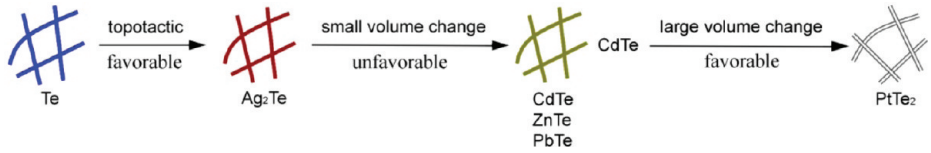

Scheme 1. Summary of the transformations investigated in this study. The as-prepared ultrathin Te nanowires were converted into Ag_2Te nanowires through topotactic transformation. The Ag_2Te nanowires were then transformed into CdTe, ZnTe, and PbTe nanowires through cation exchange. For this thermodynamically unfavorable reaction, additives were needed to increase the solubility of the reactant. Finally, the CdTe nanowires were converted into $PtTe_2$ nanotubes through a thermodynamically favorable reaction.

transformation are still in need of thorough investigation.

For transformations in one-dimensional structures, Könenkamp and co-workers demonstrated anion exchange by converting columnar ZnO into tubular ZnS with exposure to H_2S gas.[5,18] They further transformed the ZnS tubes into Ag_2S, Bi_2S_3, and Cu_2S *via* cation-exchange reactions. The tubular morphology was preserved during the transformations. Recently, we demonstrated successful transformations of Ag_2Se into CdSe while keeping the single crystallinity of the nanowires.[19,20] In addition, Yu and co-workers showed that ultrathin Te nanowires could be converted into CdTe/PbTe nanowires or Pt/Pd nanowires/nanotubes.[21,22] However, no systematic study has been carried out in nanowires for the morphological sustainability, maintenance of the single crystallinity, and preferred crystal structures during the transformations. The governing factors that should be considered for proper transformations can be summarized as the following: (i) the thermodynamic parameters that determine the transformation direction (forward or backward), (ii) the kinetics of a transformation (activation barrier), (iii) the effect of mechanical stress on retaining the initial shape, and (iv) the mechanisms of transformations (the way of diffusion for foreign cations). Alivisatos and co-workers first postulated that the solubility product of the ionic solids in the reaction medium may determine the thermodynamic direction of transformations.[15] A forward reaction is expected to occur when an ionic solid product has lower solubility than a reactant one in the reaction medium. Once the requirement is met, the kinetics can be controlled by adjusting reaction temperature to overcome the activation energy. The overall morphology of the transformed product is thought to be determined by the volume change during the reaction. Large volume change may lead to stress-induced deformation, resulting in voids or fragmentation to release the stress.[17] However, the transformation from Se nanowires into Ag_2Se has been known to preserve its shape, although they experience large volume increase. So, more study is needed for the effect of volume change on morphological sustainability. Preservation of single crystallinity requires more investigation on the transformation mechanism. The reaction may proceed homogeneously along the entire length of nanowires or initiate heterogeneously on local surfaces and form multiple grains in the end.

In this article, we executed a systematic study of chemical transformations in nanowires. We started with ultrafine, single-crystalline Te nanowires. Ultrathin nanowires have recently been a major theme of intensive research due to their high surface-to-volume ratio and unique electronic or thermal behaviors.[23,24] The large surface area and enhanced colloidal dispersion have enabled their use in sensors, catalytic supports, and solution-processable electronics.[25−27] The low dimension also led to quantum size effects, quantum conductance, and low thermal conductivities depending on the materials.[28−31] The synthesis of ultrathin nanowires has been mostly carried out by chemical methods, including template-assisted synthesis,[32,33] ligand-mediated reaction,[34,35] and intrinsically anisotropic growth.[36−38] Although the template-assisted synthesis is advantageous in terms of monodisperisty, it has difficulty in large quantity production and requires additional surface treatment to obtain stable suspensions. Ligand-mediated reactions allow scalable production as well as stable dispersion; however, mechanisms are not well-understood, which limits our control over the final crystalline structure. The intrinsic growth can generate highly anisotropic nanowires characterized by large quantity, uniform size, and stable dispersion but limited species. A typical example of such anisotropic growth can be found in chalcogens such as trigonal Se or Te.[39−44] Chemical transformations of the pristine nanowires can greatly diversify the species of nanowires. As shown in Scheme 1, the chemical transformations in this study can be divided into three groups: (i) Ultrathin Te nanowires were transformed into Ag_2Te nanowires. This transformation is a thermodynamically favorable and topotactic reaction. (ii) The Ag_2Te nanowires were converted into CdTe, ZnTe, and PbTe *via* cation exchange. The reactions are not thermodynamically favorable but may occur with small volume changes. (iii) The CdTe nanowires were transformed into $PtTe_2$, which is favorable but involves a large volume change.

RESULTS AND DISCUSSION

Synthesis of Ultrathin Te Nanowires. We prepared an aqueous solution of Te precursor (H_6TeO_6), polymeric surfactant (PVP, M_w = 55 000), and reducing agent

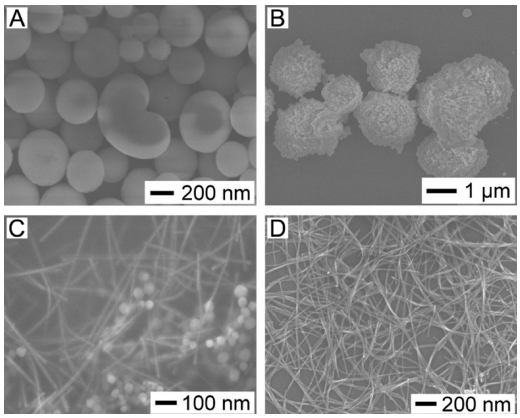

Figure 1. SEM images showing the evolution of tellurium oxide colloids into ultrathin Te nanowires: (A) tellurium oxide colloids formed right after the introduction of aqueous telluric acid into an aqueous solution of hydroxyl amine at room temperature, (B) partial dissolution of tellurium oxides at about 50 °C, (C) nucleation and growth of ultrathin *t*-Te nanowires in boiling water, and (D) the final product of ultrathin and long Te nanowires after 12 h of reaction.

(NH_2OH). SEM images in Figure 1 show a schematic flow on the formation of ultrathin Te nanowires in an aqueous solution. Shortly after the Te precursor solution was added into a mixture solution of PVP and NH_2OH, the transparent solution turned milky white, indicating the formation of spherical tellurium oxide colloids (Figure 1A).[45]

$$H_6TeO_6 + 2H^+ + 2e^- \rightarrow TeO_2 + 4H_2O,\ E^\circ = 1.02\ V \quad (1)$$

With the increase of reaction temperature to 50 °C, the spherical tellurium oxide colloids began to dissolve, which could be observed by the color change from white to dusty yellow at 50 °C. At this point, the surface of the tellurium oxide colloids became rugged (Figure 1B). The tellurium oxide(IV) was reduced to *t*-Te as the reaction temperature approached the boiling temperature of water. The dusty yellow color of the suspension changed to violet, indicating the formation of *t*-Te nanowires (Figure 1C). Complete growth of the Te nanowires needed more than 10 h under nitrogen atmosphere (Figure 1D). The Te nanowires obtained in the presence of PVP were ultrafine and had narrow distribution in their diameters. In contrast, the products prepared at the identical conditions but without PVP were very thick and largely distributed in their diameters (Supporting Information Figure S1). The control mechanism by PVP is not clear yet, but the experimental observation clearly indicates that PVP restricts the growth in thickness. Although the synthesis of Te nanowires has been reported by many researchers, our approach is novel. It is advantageous over the past reports in that the reaction is fast, very simple, and massively productive. The nanowires are ultrafine and very uniform in size. Furthermore, the process is environmentally friendly.

Figure 2A shows TEM images of the Te nanowires.

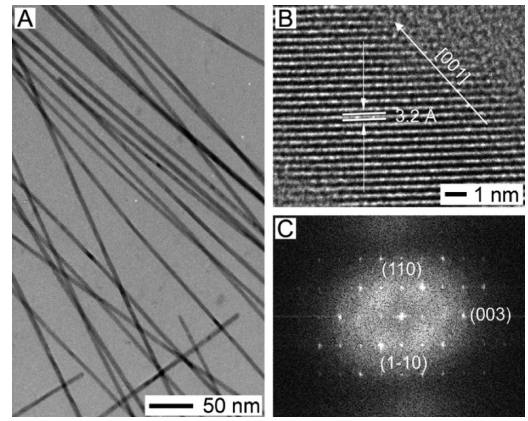

Figure 2. (A) TEM image of *t*-Te nanowires synthesized in boiling water. (B) High-resolution TEM (HR-TEM) image of the Te nanowire, which could be indexed as a hexagonal crystal structure with a lattice fringe spacing of 3.2 Å. The growth direction was along [001]. (C) Fourier transformed pattern obtained from the HR-TEM image.

They were straight and very thin with uniform diameter of 7 nm. The diameter distribution was confirmed by measuring the lateral dimensions of more than 100 nanowires in TEM images. The ultrathin Te nanowires showed a very narrow size distribution (±0.2 nm standard deviation). An HR-TEM image in Figure 2B displays the crystal lattice of a Te nanowire. The interplanar spacing was measured to be 0.32 nm, which corresponds to the separation between (101) lattice planes of hexagonal Te crystal structure. The Fourier transformed image in Figure 2C indicates that the as-synthesized nanowires have very well-defined crystal lattices. Thorough investigation with HR-TEM along the longitudinal direction of the nanowires confirmed that these ultrathin nanowires were consistently indexed as hexagonal phase structure and grown as single crystals along the [001] direction without any dislocation. We found that the average diameter of the Te nanowires was linearly decreased as the molar ratio of reducing agent to the Te precursor ($[NH_2OH]/[H_6TeO_6]$) was increased (see Figure S2 in the Supporting Information). The higher concentration of reducing agent induced higher supersaturation of Te and led to burst nucleation.

Topotactic Transformation of Te Nanowires into Ag_2Te Nanowires. It has been proven that a reaction of chalcogen with $AgNO_3$ yields silver chalcogenides.[46−49] The as-synthesized Te nanowires were redispersed in ethylene glycol with a short duration of sonication. With the

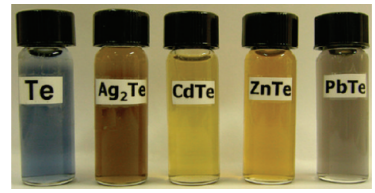

Figure 3. Photograph of methanol suspensions of Te, Ag_2Te, CdTe, ZnTe, and PbTe ultrathin nanowires obtained in this study.

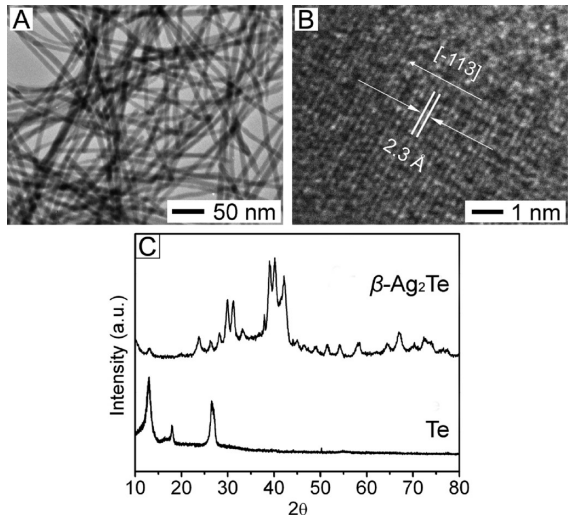

Figure 4. (A) TEM image of Ag_2Te nanowires derived from the Te nanowires. (B) HR-TEM image of the Ag_2Te nanowire. (C) XRD patterns taken from the Ag_2Te and Te nanowires. The Ag_2Te nanowires had a monoclinic structure.

dropwise addition of $AgNO_3$ solution in ethylene glycol, the deep blue suspension of Te nanowires immediately turned dark brown (Figure 3), which indicates the initiation of the conversion from Te to silver telluride nanowires. EDS analysis verified that the composition of the silver telluride nanowires was stoichiometrically correct (2:1; see the Supporting Information Figure S3).

As can be seen in the TEM images in Figure 4A, the resulting Ag_2Te nanowires preserved the structure of the original ultrathin Te nanowires. Crystal structure of the transformed Ag_2Te nanowires was characterized by HR-TEM analysis (Figure 4B). The observed interplanar spacing was about 0.23 nm, which is commensurate with the separation between (−113) lattice planes of the monoclinic β-Ag_2Te. An X-ray diffraction pattern of the Ag_2Te nanowires (Figure 4C) was also well-indexed as the monoclinic crystalline structure with a good agreement with the lattice constants from the literature data (a = 8.17, b = 8.94, c = 8.06, and β = 113°). Any byproduct such as Ag_2TeO_3 phase has not been detected with XRD, EDS, and TEM because the reaction was carried out in ethylene glycol. Since ethylene glycol reduces $AgNO_3$ into Ag atoms, the disproportionation of Te into Te^{2-} and TeO_3^{2-} is not likely to take place in the reaction.[46]

The structural preservation of the Ag_2Te nanowires is consistent to the transformation of Se nanowires into Ag_2Se nanowires. The transformation of Se was explained by the topotactic lattice matching between *t*-Se and orthorhombic or tetragonal Ag_2Se.[45] Likewise, the transformation into Ag_2Te from hexagonal Te nanowires (a = 4.46 and c = 5.93) is also in the regime of topotactic conversion, as illustrated in Figure 5. The red dots indicate Te atoms forming unit cells.

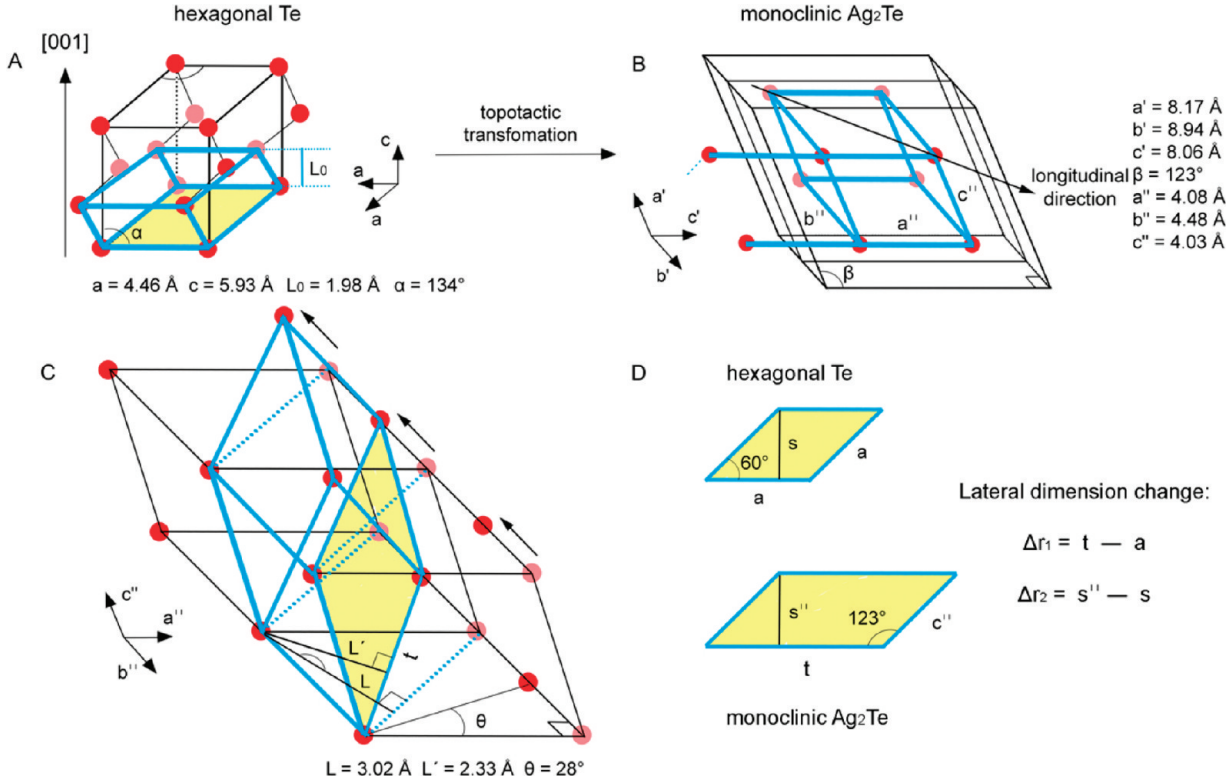

Figure 5. Schematic illustration of the crystal structures involved and definitions of the symbols. (A,B) Topotactic transformation from the helical structure of hexagonal Te into monoclinic Ag_2Te in a way that all of the lattice parameters changed. (C) Te atoms (red circles) along the a''-axis are located in a distorted way, being tilted by θ = 28° from the a'-axis (Te atoms in light-red circles). (D) Changes to lateral dimensions during the transformation from Te to Ag_2Te. Blue solid line indicates the space occupied by Te atoms, and the light yellow region is the change of lateral area of Te and Ag_2Te nanowires.

TABLE 1. Lattice Parameters of 8 Unit Te Atoms and Their Volumes before and after Transformation from Te into Ag_2Te

	hexagonal Te (Figure 5A, black solid line)	monoclinic Ag_2Te (Figure 5B, black solid line)	reduced Ag_2Te (Figure 5B, blue solid line/Figure 5C, black solid line)
lattice constants	$a = 4.46$, $c = 5.93$, $\alpha = 134°$	$a' = 8.17$, $b' = 8.94$, $c' = 8.06$, $\beta = 123°$	$a'' = 4.08$, $b'' = 4.48$, $c'' = 4.03$
unit cell volume	102.3 (Å^3)	271.4 (Å^3)	67.8 (Å^3)
volume occupied by 8 Te atoms	34.1 (Å^3)	67.8 (Å^3)	67.8 (Å^3)

Such transformation normally requests small structural change during the reaction. In spite of the severe volume increase in the transformation of Se into Ag_2Se, the overall structure was well-maintained and even the single crystallinity was conserved. This is not well-understood. This part investigates how the structure of Se or Te can be reserved by examining the increase of the length instead the overall volume increase. In the reaction, the direction along the major axis of the monoclinic Ag_2Te nanowires is not equivalent to the *c*-axis of the hexagonal Te nanowires. The [001]-directed hexagonal Te was transformed into [110]-directed monoclinic phase. Thus, the [001] direction of Te and [110] direction of Ag_2Te are major axes of Te and Ag_2Te nanowires. This is because the Te atoms in the *a*-, *b*-, and *c*-axis in the Te nanowires do not belong to the atomic position in the axis a', b', and c' in the Ag_2Te nanowires. The monoclinic Ag_2Te has the four-fold general position of all atoms in its unit cell. The Te atoms positioned along the a''-axis exist in a distorted way, being tilted by $\theta = 28°$ from the a'-axis, as demonstrated by Frueh[50] (solid arrow in Figure 5C). After the transformation, the relative position of the 8 Te atoms in the Te nanowires changed as follows: 4.46 to 4.08 Å, 4.46 to 4.48 Å, and 1.98 to 4.03 Å, respectively (a to a'', b to b'', c to c''). Thus, the volume change can be obtained by calculating the volume difference of Te and resulting Ag_2Te occupied by 8 Te atoms (blue solid line, Figure 5). From simple mathematics (eq 2), the volume change was calculated to be $\Delta V/V = 0.9882$. This calculation is quite consistent with the calculation obtained from the density and molecular weight of Te and Ag_2Te, which is $\Delta V/V = 1.010$ (eq 3).

$$\Delta V/V = [V_{Ag_2Te} - V_{Te}]/V_{Te} \quad [V_{Ag_2Te} = a'' \times b'' \times c'' \times \sin(180° - \beta),\ V_{Te} = a \times a \times \sin 60° \times 1/3 \times c] \quad (2)$$

$$\Delta V/V = [V_{Ag_2Te} - V_{Te}]/V_{Te} \quad [V_{Te} = M_{Te}/\rho_{Te},\ V_{Ag_2Te} = M_{Ag2Te}/\rho_{Ag_2Te}] \quad (3)$$

The increase in the lattice constant of the major axis ($\Delta L = L - L_o$) between the Te and Ag_2Te nanowires yields the value of 1.04 Å, which is a 52% increase. However, due to the tilted angle of the a''-axis from the a'-axis of Ag_2Te ($\theta = 28°$), the actual contribution to the increase in actual length of the nanowires is much smaller, 17% (L'/L_o, $\Delta L = L' - L_o$), that is, 0.35 Å. Therefore, considerable amount of volume increase came from the increase of the lateral dimension of the nanowires. The lattice parameters of 8 unit Te atoms and their volumes before and after transformation are listed in Table 1. The lateral dimension difference between Te and Ag_2Te can be divided into two directions.

$$\Delta r_1 = t - a = [(a'')^2 + (3/2b'')^2]^{1/2} - a,\ \Delta r_1/a = 0.76 \quad (4)$$

$$\Delta r_2 = s'' - s = a \times \sin 60° - 4.03\ \text{Å} \times \sin(180° - \beta),\ \Delta r_2/a = -0.04 \quad (5)$$

Δr_1 is the change between the *a*-axis of Te and the [110] direction of Ag_2Te, which is comparable to 3.4 Å or 76% increase (eq 4). The Δr_2 is the difference between the *a*-axis of Te and the c''-axis of Ag_2Te, which is 0.15 Å or 4% decrease (eq 5). From the above calculation, the volume change during the transformation from hexagonal Te to monoclinic Ag_2Te is estimated as 98% ($\Delta V/V = (1 + 0.17) \times (1 + 0.76) \times (1 - 0.04) = 0.9768$), which is consistent with the values calculated with the volume occupied by 8 Te atoms. It should be noted that the 17% increase in the actual length during the transformation is much smaller than expected from the severe volume increase. However, the mechanical stress accumulated during the transformation is too much for the nanowires to absorb in their structure. The stress was relieved by breaking the nanowires, producing shorter nanowires. In our experiment, the initial Te nanowires (longer than 10 μm) were shortened to 1−2 μm. The resulting Ag_2Te nanowires were found to be single crystalline. The preservation of the single crystallinity indicates that the transformation took place in a homogeneous way along the entire length of the Te nanowires. If heterogeneous nucleation and growth along the nanowires took place, it would generate multiple small grains with rough surface topology.

Structural conservation of the Te nanowires after transformation into Ag_2Te in spite of the 100% volume increase is surprising. In order to experimentally monitor the dimensional change in length and diameter during the transformation from Te to Ag_2Te, we performed the transformation starting from Te nanorods instead of Te nanowires. Figure 6 shows SEM images of the Te nanorods synthesized in ethylene glycol (EG) at 100 °C with sodium tellurite as a precursor (A) and Ag_2Te nanorods (B) converted from the as-synthesized Te nanorods through topotactic reaction in EG. HR-TEM analysis was used to check the crystal structures of the Te and

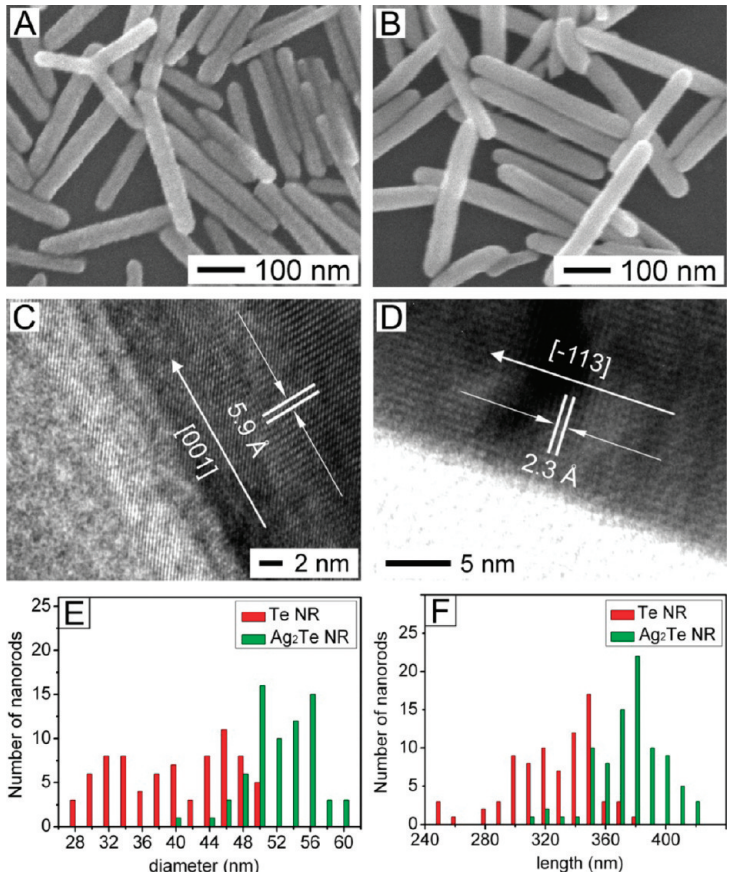

Figure 6. SEM and HR-TEM images of (A,C) Te nanorods synthesized in ethylene glycol (EG) at 100 °C for 2 h and (B,D) Ag_2Te nanorods derived from the as-synthesized Te nanorods through a topotactic reaction with $AgNO_3$ in EG. (E) Ag_2Te nanorods had an average diameter of 52 nm, corresponding to a 33.3% increase relative to the Te nanorods (d = 39 nm). (F) Average length of Ag_2Te nanorods increased by 14% as compared to that of Te nanorods.

Ag_2Te nanorods. As seen in the ultrathin nanowires, the growth direction of Te nanorods was [001] and the Ag_2Te nanorods were grown along [−113]. The lattice spacing of Ag_2Te nanorods along the axial direction was 0.23 nm, which is consistent with the calculated result. Figure 6E shows the distribution in diameter of the Te and Ag_2Te nanorods. The average diameter of Ag_2Te nanorods was about 52 nm increased. From the average diameter of the Te nanorods (39 nm), 13 nm increase (33% increase) was monitored. Figure 6F gives the distribution in the length of the Te and resultant Ag_2Te nanorods. Average length of the Ag_2Te nanorods was 337 nm, which is 48 nm larger than the value of Te nanorods. The length change shows 14% increase. From the experimental data, the average volume expansion can be calculated as follows: $\Delta V = (1 + 0.333) \times (1 + 0.333) \times (1 + 0.140) = 2.0256$ and $\Delta V/V = 1.0256$. This experimental result is consistent with the calculated volume expansion from Figure 5.

Thermodynamic Determination of Favorable Direction in Cation-Exchange Reactions. Since Son *et al.* reported on the cation-exchange reactions in chalcogenide nanocrystals,[15] various researchers have explored the transformation to prepare other nanomaterials. As Wark and Son pointed out in their recent paper,[17] we should consider three important factors to fully take advantage of the cation-exchange reaction: solubility of ionic solids, crystal structure, and mechanical stress generated by volume change during the reaction. The difference in solubility product of the reactants and products can be chosen as the first criterion to determine the thermodynamically favorable direction in the cation exchange. Solubility product, K_{sp}, of ionic solid is referred to as an equilibrium constant between an ionic solid and its dissolved state in solution. The equilibrium solubility constant (K) is a product of activities of each constituent chemical. When the solubility or concentration of the salt is very low, which is the case for most inorganic synthesis, the activity can be taken as the concentration of the constituting ions. Solubility product is related to the free energy change of a solution ($\Delta G = -RT \ln K_{sp}$), which leads to a conclusion that an ionic solid with a relatively high K_{sp} value goes through cation exchange to form another ionic solid with a relatively low K_{sp}. Of course, the solubility product approach cannot provide the exact solvation of the ionic solids in the reaction conditions because actual solubility is affected by many other factors even without changing the solubility product values. Addition of a common ion with the ionic solid can shift the solubility equilibrium. Even noncommon salts can affect the ionic strength of the solution to alter the solubility of ionic solids without changing the solubility products. Temperature is a basic parameter to change the solubility of ionic solids. Temperature rise can increase the solubility for an endothermic dissociation process and can decrease for an exothermic process. The solubility may differ according to the crystal structure of ionic solids with the same stoichiometry, even though the difference is usually not large. When the size of materials goes down to nanoscale, the solubility is greatly increased. The effect can be quantified as follows:[51]

$$\log K^*_{sp} = \log K_{sp,bulk} + 2\gamma A_m/[3\log(RT)] \qquad (6)$$

where K_{sp}, γ, and A_m are the solubility product, the surface tension, and the molar surface area (in m^2/mol) of the solute in the order. Therefore, ultrathin nanowires or nanocrystals should possess enhanced solubility compared with bulk materials, which should result in the fast reactions as observed.[15,17] The existence of complexation species to the constituting ions can considerably increase the solubility without changing the solubility product itself because the complexed form does not enter the solubility equilibrium. When the dimension of the reactant nanowire is fixed at a limited range of reaction

TABLE 2. Solubility Product Data of Various Metal Chalcogenides in Descending Order

	Solubility Product Constant, K_{sp} at 25 °C						
solid	E = S	E = Se	E = Te	solid	E = S	E = Se	E = Te
Ag_2E	3×10^{-50}	1×10^{-54}	N.A.	NiE	1×10^{-21}	2×10^{-26}	N.A.
Bi_2E_3	1×10^{-100}	1×10^{-130}	N.A.	PbE	1×10^{-28}	1×10^{-37}	N.A.
CdE	1×10^{-28}	4×10^{-35}	1×10^{-42}	PtE	9.9×10^{-74}	N.A.	N.A.
CuE	5×10^{-36}	2×10^{-40}	N.A.	SbE	2×10^{-93}	N.A.	N.A.
HgE	6×10^{-53}	4×10^{-59}	N.A.	SnE	1×10^{-26}	5×10^{-34}	N.A.
In_2E_3	6×10^{-76}	N.A.	N.A.	ZnE	3×10^{-25}	1×10^{-27}	N.A.

temperature, proper choice of salts and complexing agents may be good variants to alter the direction of cation exchange. Strong complexation of organic additives with the cations in the reactant solid as well as introduction of anions having good miscibility with the same cations can selectively increase the solubility of the cations, which, in turn, can cause the backward reaction to occur. The concept has been already proven in the cation-exchange reaction from Ag_2Se into CdSe. In the presence of $(NO_3)^-$ anions from the $Cd(NO_3)_2$ precursor, the backward reaction could be accomplished only when complexation additives (TBP or TOP) existed in the solution. Although phosphines in alcohols or aqueous solutions can be oxidized into phosphine oxides or phosphorus acids, the oxidation does not have considerable effect on the overall cation-exchange reactions because the oxides also can bind to the cations in the lattice and form intermediate complexes to facilitate the exchange by other cations. Since dissociation of most chalcogenide semiconductors is an endothermic process, temperature rise will increase the solubility of both reactant nanowires and transformed nanowires. Therefore, temperature change may not be effective to alter the thermodynamic direction of the cation exchange, but rather accelerate the exchange rate in forward reactions. Here, we can raise another question: if a cation exchange is thermodynamically favored, what determines the crystal structure of the final product? Although the solubility products are different according to the crystal structure, the difference is not high enough to determine the resulting ionic crystals. We will mention later that the crystal structure is determined in the way to minimize the free energy of formation, ΔG_f, during the transformation.

Table 2 shows literature values of the solubility product of metal chalcogenides in water in descending order.[52−54] Although solubility products of metal sulfides in water were readily found from the literature, full data of all chalcogenide compounds, especially metal tellurides, were not obtainable. However, qualitative K_{sp} values can be estimated considering the molar enthalpy of solvation (ΔH_{solv}).

$$M^+X^-(s) \rightarrow M^+(aq) + X^-(aq); \Delta H_{solv}[M^+X^-(s)] \quad (7)$$

$$M^+(g) + X^-(g) \rightarrow M^+X^-(s); \Delta H_{latt}[M^+X^-(s)] \quad (8)$$

$$M^+(g) \rightarrow M^+(aq); \Delta H_{hyd}[M^+(g)] \quad (9)$$

$$X^-(g) \rightarrow X^-(aq); \Delta H_{hyd}[X^-(g)] \quad (10)$$

$$\Delta H_{solv} = \Delta H_{hyd} - \Delta H_{latt} \quad (11)$$

Both the lattice enthalpy (ΔH_{latt}) and hydration enthalpy (ΔH_{hyd}) are negative values. A high lattice enthalpy means an insoluble compound, while a high hydration enthalpy for an ion indicates a soluble compound. Negative value of solvation enthalpy indicates exothermic dissolution, and positive value shows an endothermic process. The lattice enthalpy is inversely proportional to the summation of the radii of the constituting ions, $1/(r^+ + r^-)$, while the total hydration enthalpy, with each ion being hydrated individually, is the sum of individual ion's contribution ($1/r^+ + 1/r^-$). As the size of anion is increased for a same cation species, the decrease of hydration enthalpy is larger than that of lattice enthalpy because radius change cannot make the denominator small by itself in the lattice enthalpy. So we can make a conclusion that solubility products of metal chalcogenides have a lower value as the ionic radius of chalcogen increases: $K_{sp}(M_xS_y) > K_{sp}(M_xSe_y) > K_{sp}(M_xTe_y)$. As shown in Table 1, K_{sp} values of M_xSe_y are lower by 10^3-10^8 than corresponding M_xS_y, and the same rule of thumb may be applied between M_xTe_y and M_xSe_y. For example, the solubility product of CdS, CdSe, and CdTe is in the order as follows: K_{sp} (CdS) $= 10^{-28}$, K_{sp}(CdSe) $= 10^{-35}$, and K_{sp}(CdTe) $= 10^{-42}$. With this general tendency on the solubility of chalcogenides, we can assume that metal tellurides also have the same trend with the solubility products of metal sulfides.

For the cation-exchange reactions in this study, methanol and ethylene glycol were used as solvents. The solubility product (K_{sp}) will change if the solvent is different from water. Unfortunately, the solubility data of chalcogenides in alcoholic solutions are not available. Generally, organic solvents have lower capacity to dissolve ionic solids since their dielectric constants are usually smaller than that of water. Nevertheless, we believe it is a reasonable approach to use the K_{sp} value in aqueous solutions as the rough criterion to determine the direction of exchange reactions, especially for sol-

vents with rather high dielectric constants such as alcoholic solutions. Ions in a polar solvent interact with the solvent molecules *via* ion−dipole interactions. For solvents such as water, the interaction between ions and solvents is energetically favorable. In regard to this, we think the K_{sp} values of ionic solids in nonaqueous polar solvents do not have significant deviation from the trend in aqueous solutions. On the basis of the known K_{sp} values of metal sulfides in water, the metal tellurides studied in this work can be categorized into three groups. The first group includes CdTe, ZnTe, and PbTe that have the highest K_{sp}. The solubility products between them are not expected to have a large difference. The second one is silver telluride with medium range of K_{sp} compared to the other two groups. The last one would be tellurides with very lower K_{sp}, which correspond to $PtTe_2$. The comparison of K_{sp} values indicates that the transformations from most metal chalcogenides into $PtTe_2$ are thermodynamically favored, while the transformations from Ag_2Te into ZnTe, CdTe, and PbTe are not allowed in pure solvents.

Transformation of Ag_2Te Nanowires into MTe (M = Cd, Zn, Pb): Unfavorable Reaction with Small Volume Change. Several studies have employed the silver chalcogenide nanostructures for further transformation into other metal chalcogenides such as CdE, ZnE, PbE, Cu_2E, Sb_2E, and Bi_2E_3 (E = S, Se, and Te).[18,55] The unfavorable reaction has been known to be enabled with the aid of ligands such as trioctylphosphine (TOP) and tributylphosphine (TBP), which can form a complex with Ag^+, selectively increasing the solubility product of Ag_2Te in the solution.

$$M^+(aq) + L \rightarrow (ML)^+ \quad \Delta H_{complx} = \Delta H[(ML)^+(aq)], \quad L = \text{ligand} \qquad (12)$$

$$\Delta H_{solv} = \Delta H_{hyd} - \Delta H_{latt} + \Delta H_{complx} \qquad (13)$$

For the transformation from CdTe to Ag_2Te, no thermal heating or ligand addition were needed and the reaction was very fast.[15] There are two criteria that should be taken into consideration in determining the direction of plausible reaction. First, the reaction occurs in a direction of lower activation energy. The experimentally determined rate constant (k) for Ag_2Te to CdTe is much smaller than the rate constant (k') for CdTe to Ag_2Te. The large difference in the rate constant gives almost no transformation into CdTe in pure solvent at low temperature. The difference in the rate constant means that the activation energy for the reaction from Ag_2Te to CdTe is much higher than the reverse reaction, which, in turn, shows that the energy of Ag_2Te is lower than that of CdTe. Large addition of Cd^{2+} ions at the conditions of reduced activation energy (addition of the ligands) and increased thermal energy makes it possible for the reverse reaction to take place. In addition to the kinetic barrier, the direction of reaction is determined by the relative thermodynamic stability of product with respect to reactant, which corresponds to the difference of free energy change. In our experiments, the as-synthesized Ag_2Te nanowires were redispersed in methanol, followed by the addition of methanol solution of $Cd(NO_3)_2$, $Zn(NO_3)_2$, and $Pb(NO_3)_2$ at 50 °C. It is worth noting that a small amount of water was indispensable for the case of $Pb(NO_3)_2$ due to its low solubility in methanol.[16] The dark brown Ag_2Te nanowire suspension in methanol showed no reaction in the presence of metal nitrate precursors. However, the reaction took place right after the quick injection of TBP and turned to light yellow (CdTe), light red (ZnTe), and light gray (PbTe) (see Figure 3). SEM images in Figure S5 (Supporting Information) show that the resulting metal telluride nanowires obtained by cation-exchange reaction kept their long and ultrathin nanowire morphology. EDS measurement was used to check the stoichiometry of those nanowires, which confirmed exact 1:1 stoichiometric coincidence between metal and Te (see Figure S3 in the Supporting Informations). Figure 7 is the X-ray diffraction patterns of metal telluride nanowires transformed from the Ag_2Te nanowires. The patterns characterized the three types of nanowires as a cubic crystal structure: zinc blende (CdTe and ZnTe) and NaCl-type (PbTe). Figure 8 demonstrates TEM images of the transformed metal telluride nanowires. All of the nanowires turned out to preserve the initial morphology of the Ag_2Te nanowires. The crystal lattices of the nanowires obtained from HR-TEM micrographs were also indexed as zinc blende for CdTe, ZnTe, and NaCl-type cubic structure for PbTe nanowires. HR-TEM image in Figure 8B shows that CdTe nanowires have interplanar spacing of 0.37 and 0.23 nm, which corresponds to the separations between (111) and (220) of the zinc blende crystal structure. It should be noted that a majority of the CdTe nanowires had the zinc blende crystal structure, while some nanowires showed wurtzite structure, which can be confirmed by zigzag morphology, as shown in Figure 9. The XRD analysis also indicates the admixture of wurtzite and zinc blende structures, which results in the peak broadening in CdTe and ZnTe nanowires (arrowed in Figure 7). This phase admixture of two different types of crystalline structure has already been reported by Kuno group.[56] They found

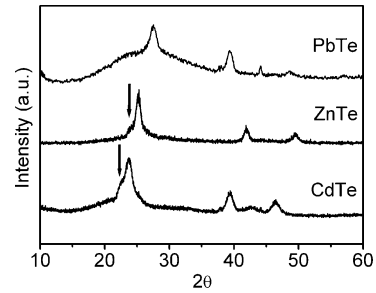

Figure 7. XRD data of CdTe, ZnTe, and PbTe nanowires derived from Ag_2Te nanowires. The majority of nanowires had a cubic crystal structure: zinc blende (CdTe and ZnTe) and NaCl-type (PbTe). The arrows indicate peaks from the wurtzite crystal structure of CdTe and ZnTe.

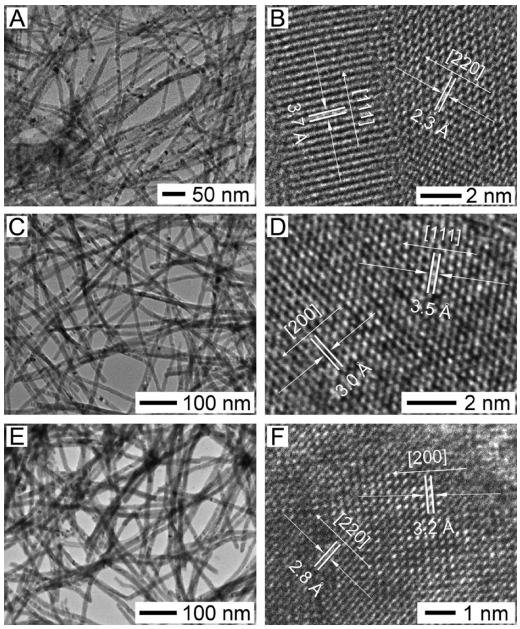

Figure 8. TEM and HR-TEM images of (A,B) CdTe, (C,D) ZnTe, and (E,F) PbTe nanowires derived from Ag_2Te nanowires. Since the reactions were not spontaneous in pure methanol, tributylphosphine (TBP) was added and the reaction was performed at 50 °C for 1 h. The morphology and single crystallinity of reactant Ag_2Te nanowires were well-preserved after the transformation.

that local positions of twinning and mixed phase (zinc blende/wurtzite) are identified with characteristic "zigzag" fringes in lattice-resolved TEM images. In ZnTe nanowires in Figure 8D, the interplanar spacings were observed as 0.3 and 0.35 nm, indicating the direction of (200) and (111), respectively. HR-TEM image of a PbTe nanowire in Figure 8F revealed the interplanar distance of 0.28 and 0.32 nm for the spacing between planes of (220) and (200), respectively.

In the solution-based synthesis of nanostructured binary materials, zinc blende and wurtzite structure are frequently observed. The transformed CdTe, ZnTe, and PbTe showed mostly cubic crystal structures even though a mixture of the two structures is expected due to the small difference in solubility products between the two structures. Table 3 summarizes the volume change during the transformation in this study according to the expected crystal structures. The difference of free energy of formation, ΔG_f, between

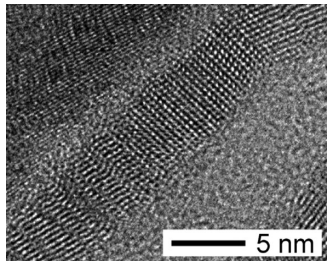

Figure 9. HR-TEM image of individual CdTe nanowires showing the admixture of zinc blende and wurtzite crystal structure. Most nanowires were zinc blende, but a small portion of them appeared as a the mixed structure.

TABLE 3. Structure, Lattice Parameters, and Volume Change during Chemical Transformations in This Study

initial material		final product	$\Delta V/V$
Te	Ag_2Te	monoclinic	1.009
trigonal		$a = 8.17, b = 8.94, c = 8.06$	
$a = 4.46, c = 5.93$			
Ag_2Te	CdTe	zinc blende	0.0025
		$a = 6.48$	
		wurtzite	0.0036
		$a = 4.57, c = 7.44$	
	ZnTe	zinc blende	−0.163
		$a = 6.10$	
		wurtzite	−0.1599
		$a = 4.31, c = 7.09$	
	PbTe	cubic	−0.0076
		$a = 6.45$	
		orthorhombic	−0.1413
		$a = 4.7, b = 12.1, c = 4.1$	
CdTe	$PtTe_2$	hexagonal	−0.462
		$a = 4.02, c = 5.22$	

two structural phases (CdTe, ZnTe, and PbTe) should be taken into account to determine the preferred phase in the product. In the transformation from Ag_2Te into PbTe, conversion into a cubic structure (NaCl-type, ambient phase) has a small volume decrease while the orthorhombic structure (high-pressure phase) experiences large volume decrease, which resulted in the product with cubic crystal structure exclusively obtained in our experiment. That is because free energy of formatin of cubic PbTe is less than the high-pressure phase in ambient condition, which is under thermodynamic control.[57,58] In the case of CdTe and ZnTe transformation, however, there should be no special preference for zinc blende and wurtzite in light of a very small difference of free energy of formation between wurtzite and zinc blende structure (7.0 and 6.4 meV for CdTe and ZnTe, respectively).[60] Nevertheless, the major crystal structure of resultant CdTe and ZnTe nanowires was found to be zinc blende, although a small portion of wurtzite-structured products was observed. We consider that the zinc blende phase is the major product due to its better stability at relatively low temperatures.[59,60] The degree of volume change during the exchange reaction can be considered as a means to predict the easiness of the chemical transformation. We consider that cation exchange resulting in small volume change leads to faster transformation. Comparing the volume change between the cubic structure of CdTe and ZnTe, volume decrease in ZnTe is larger than that in CdTe. This difference was reflected in the reaction time for full conversion. While the full conversion from Ag_2Te into CdTe and PbTe took only a couple of minutes, transformation into ZnTe required more than 10 min at the identical conditions. It implies that the necessary reaction time would increase in transformations accompanying a relatively large volume change. It is noticeable that we could not detect

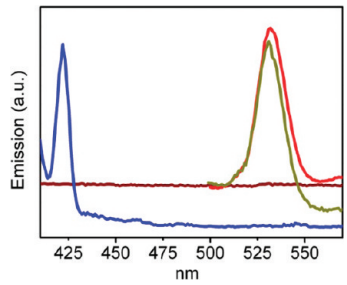

Figure 10. Photoluminescence spectra taken from Te (blue), Ag_2Te (brown), CdTe (dark yellow), and ZnTe (red) nanowires.

length change between the reactant Ag_2Te nanowires and the product CdTe, ZnTe, and PbTe nanowires.

Emission spectra of the Te, Ag_2Te, CdTe, and ZnTe nanowires in solution are provided in Figure 10. The dispersion of ultrathin Te nanowires in aqueous medium exhibits a deep blue color, which is substantially different from thick Te nanowires (gray color) with several tens of nanometers in diameter synthesized in other synthetic routes. In this respect, the ultrathin Te nanowires have unique optical properties compared to the bulk counterpart. Currently, it is not determined if the origin of the peak at 420 nm is from the allowed direct transition from the valence band (p-type lone-pair triplet) to the conduction band (p-antibonding triplet)[61] or from the surface plasmon.[62] The Te nanowires lost their emissive characteristics after the transformation into Ag_2Te nanowires, which have very low band gap energy (~0.1 eV at 300 K). The maximum emission of the CdTe nanowires in dispersion appeared at around 531 nm with an excitation wavelength of 400 nm (dark yellow curve). The ZnTe NW in dispersion showed the maximum emission peak at around 532 nm with an excitation wavelength of 400 nm.

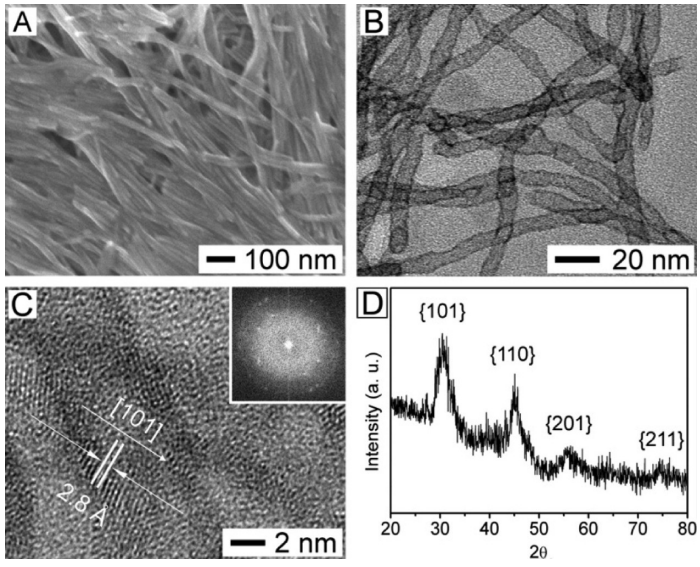

Figure 11. (A) SEM and (B) TEM images of $PtTe_2$ nanotubes derived from CdTe nanowires through a cation-exchange reaction in methanol at room temperature. (C) HR-TEM image of a $PtTe_2$ nanotube indexed as the hexagonal phase with lattice spacing of 0.28 nm along the [101] direction. The inset shows the Fourier transformed ring pattern of $PtTe_2$ nanotubes. (D) XRD of the $PtTe_2$ nanotubes. All peaks were indexed to a hexagonal crystal structure for $PtTe_2$.

Transformation from CdTe into $PtTe_2$: Favorable Reaction with Large Volume Change. For investigation on the cation-exchange reaction that does not require any complexation additives, so-called the forward cation-exchange reaction, we adopted CdTe nanowires as an initial material. We washed CdTe nanowires with methanol several times by centrifuge and redispersed the precipitate in toluene for the cation exchange with Pt^{4+} (H_2PtCl_6). It is worthy to note that the surface of CdTe nanowires was modified with ligands such as trioctylphosphine oxide (TOPO) to fully disperse them in toluene. The transformations are expected to experience large negative volume change ($\Delta V/V_o$), as indicated in Table 3. As previously studied by Son and co-workers, relatively large volume change during the ion-exchange reaction should accompany various effects on the morphology of the final product. While the preservation of single crystallinity was observed in the reaction from Ag_2Te into M_xTe_y, in which the volume change was not large, the single crystal structure of the CdTe NW was barely conserved during the transformation into $PtTe_2$ due to the severe volume change. The mechanical stress accumulated inside the structure prevents the formation of single domain crystals spanning long distance. The accumulated stress should be released by forming a different morphology in the product. We observed that the product after the cation-exchange reaction of the CdTe nanowire with Pt^{4+} was $PtTe_2$ nanotube, as exhibited in Figure 11. Since H_2PtCl_6 is not reduced in toluene or methanol to form pure Pt particles, the reaction does not necessarily to generate other heterostructures. Unlike the Kirkendall effect caused by the difference of diffusion flux between two chemical species, the formation of void in product morphology was induced to release the mechanical stress accumulated during the reaction. The anion sublattice has the key in the morphology of the final product in the cation-exchange reaction. The Te atoms moved to the surface to release the stress accumulated at the surface region as the transformation proceeded from the surface. The transformation took only a few seconds due to the large difference in the solubility products between CdTe and $PtTe_2$. As can be seen in the TEM image (Figure 11B,C), the wall thickness of the $PtTe_2$ nanotubes was in the range of 1−2 nm. The voids in the $PtTe_2$ nanotube were continuous, as can be seen in Figure 11B. The HR-TEM image obtained from one $PtTe_2$ nanotube indicates they are polycrystalline. There was no preferred orientation of the grains in the $PtTe_2$ nanotube. The lattice fringe was indexed as the interplanar spacing of 0.28 nm in the direction of [101]. The large volume change can require rapid release of the stress in every direction, which results in the polycrystalline structure of $PtTe_2$, confirmed by ring patterns of the Fourier transformed image (inset in Figure 11C). The XRD pattern in Figure

11D shows that the $PtTe_2$ nanotubes are indexed as a hexagonal crystal structure, which is consistent with the literature (JCPDS card 88-2277). We believe that the peak broadening in the $PtTe_2$ nanotubes was caused by the voids and small grains. EDS result also indicates a 1:2 stoichiometric composition (Supporting Information Figure S7).

CONCLUSION

We have systematically studied the chemical transformation in various ultrathin metal telluride nanowires M_xTe_y (M = Ag, Cd, Zn, Pb, and Pt). The results can be summarized as follows. First, the solubility product of ionic solids can be a rough, but useful, criterion to anticipate if the transformation is thermodynamically favorable or not. The transformations from CdTe into $PtTe_2$ were found favorable in pure solvents because the solubility products of $PtTe_2$ were much lower than that of CdTe. Meanwhile, the transformations from Ag_2Te into CdTe, ZnTe, and PbTe were unfavorable in pure solvents. The reactions required complexation additives to initiate the conversion. Second, the morphological preservation of reactant nanowires is dependent on the dimensional change in length direction rather than total volume change. The small amount of volume change from Ag_2Te nanowires into CdTe, ZnTe, and PbTe led to well-preserved single crystalline naowires. In the topotactic transformation between Te and Ag_2Te nanowires, the large volume increase (100%) was attributed to the expansion in the lateral direction rather than in the length, resulting in smaller mechanical stress in the nanowires than expected from the volume increase. As a result, the transformation shortened the long Te nanowires (>10 μm) to 1−2 μm, instead of severe chopping. In contrast, considerable volume change without lattice matching in the transformation from CdTe to $PtTe_2$ led to nanotubes due to the accumulation of mechanical stress. Third, crystal structure in the transformation should be determined in a way to minimize the free energy of formation. Lattices accompanying a lower ΔG_f value took the majority in the crystal structures of the transformed nanowires. In the transformation from Ag_2Te to PbTe, all of the crystal structures were selectively NaCl-type cubic, not orthorhombic. This is because the orthorhombic lattice of the high-pressure phase has a larger ΔG_f value. In the case of CdTe and ZnTe, there is little difference in free energy of formation between zinc blende and wurtzite phase, which may result in an admixture of the two crystal structures. Nonetheless, the major crystal structure of the products was zinc blende due to better stability of the phase at low temperatures over the wurtzite phase. This observation indicates that the stability of the products is another factor to determine the crystal structures. Fourth, the reactions with small volume change or good lattice matching are considered homogeneous; on the other hand, reactions with a large volume change without lattice matching take place heterogeneously. The small volume change in the transformation from Ag_2Te into CdTe, ZnTe, and PbTe nanowires led to single crystalline metal tellurides, which is only possible through homogeneous reactions along the entire length of the nanowires. In contrast, the transformation from CdTe into $PtTe_2$ was governed by heterogeneous conversion and resulted in fragmented domains. Although we need more studies on the transformation mechanism and exact solubility of ionic solids, the results in this study may be used as a first guide to the chemical transformations between nanostructured materials.

EXPERIMENTAL SECTION

Materials. The chemicals used in this study were telluric acid (H_6TeO_6, ≥97.5%, Aldrich), sodium tellurite (Na_2TeO_3, 99%, Aldrich), hydroxylamine (NH_2OH, 50 wt % in H_2O, Aldrich), L(+)-ascorbic acid ($C_6H_8O_6$, Shinyo pure chemicals), poly(vinyl pyrrolidone) (PVP, $M_w \approx$ 55 000, Sigma-Aldrich), silver nitrate ($AgNO_3$, 99.0%, Fluka), cadmium nitrate ($Cd(NO_3)_2$, 98%, Aldrich), zinc nitrate ($Zn(NO_3)_2$, 98%, Sigma-Aldrich), lead nitrate ($Pb(NO_3)_2$, 99.999%, Aldrich), hydrogen hexachloroplatinate (H_2PtCl_6, 99.9%), methanol (J.T. Baker, Lot G37E18), ethylene glycol (EG, ≥99%, Sigma-Aldrich, batch number 10196HK), toluene (99.9%, J.T. Baker, Lot H18N51), trioctylphosphine oxide (TOPO, technical grade, 90%, Aldrich, batch number 06520ED), and tributylphosphine (TBP, tech. 90%, Aldrich, batch number 06202PC). The deionized water used for the synthesis of Te nanowires was obtained using an 18 MΩ (SHRO-plus DI) system.

Synthesis of Te Nanowires. Aqueous telluric acid solution (0.5 g in 50 mL of DI water) was added into a mixture of aqueous PVP solution (1.0 g in 50 mL of DI water) and hydroxylamine aqueous solution (0.9−2.4 mL in 20 mL of DI water) in a 250 mL round-bottom flask under magnetic stirring at room temperature. The reaction system was sealed and set to 95 °C under nitrogen (N_2) environment. In a few seconds, the color of the solution became milky white, which indicates the formation of tellurium oxide colloids. The color of the tellurium oxide suspension gradually turned dark gray. Complete growth of the Te nanowire took about 12 h and could be confirmed by the deep blue color.

Transformation of Te Nanowires to Ag_2Te Nanowires. The suspension of as-synthesized Te nanowires was centrifuged three times with addition of volumetric water twice, and the supernatant was decanted. The collected Te nanowires were redispersed in EG. Addition of silver nitrate (0.1 g) solution into the EG suspension under vigorous stirring at room temperature immediately transformed the Te nanowires to Ag_2Te nanowires. During the reaction, the color of the suspension changed from deep blue to brown. The reaction was allowed to proceed for 1 h for complete transformation. The Ag_2Te nanowires were collected after three cycles of centrifugation and washing with DI water.

Synthesis of Te Nanorods and Their Transformation to Ag_2Te Nanorods. A sodium tellurite solution in EG (0.5 g in 50 mL) was injected into a mixed solution of PVP (2 g in 50 mL of EG) and ascorbic acid (0.3 g in 30 mL of EG) in a 250 mL round-bottom flask under vigorous stirring at room temperature. The reaction system was set at 100 °C under ambient pressure. In 2 h, the color changed to black, indicating the formation of Te nanorods. A small amount of Te nanorods was redispersed in ethylene glycol after three cycles of centrifugation and washing. Silver nitrate solution (0.1 g in 5 mL EG) was added into the suspension of Te nanorods at room temperature. The color of the suspension changed brown within a few minutes, suggesting that the trans-

formation from Te to Ag_2Te was complete. The Ag_2Te nanorods were washed with water several times for characterization.

Cation-Exchange Reaction for Transforming Ag_2Te into MTe (M = Cd, Pb, and Zn). The Ag_2Te nanowires were redispersed in methanol (10 mL) for the cation-exchange reaction. Cadmium nitrate (40 mg), zinc nitrate (40 mg), and lead nitrate (35 mg) solution in methanol (3 mL)—a small amount of water was necessary to dissolve lead nitrate—were added into the Ag_2Te nanowire suspension in methanol. The reaction temperature was set at 50 °C under vigorous stirring. Then, 0.2 mL of tributylphosphine (TBP) was injected. The reaction was fast enough so that the color of the suspension changed to light blue (CdTe), light red (ZnTe), and indigo blue (PbTe) in a few minutes.

Cation-Exchange Reaction for Transforming CdTe Nanowires into $PtTe_2$ Nanotubes. The CdTe nanowires transformed from Ag_2Te nanowires were dried in a desiccator and then redispersed in toluene (10 mL). To achieve complete dispersion of CdTe nanowires, trioctylphosphine oxide (TOPO, >1 g) was added into the toluene suspension and the suspension was ultrasonicated for 30 min. Then, for the transformation into $PtTe_2$, a solution of hydrogen hexachloroplatinate (H_2PtCl_6, 50 mg) in methanol (5 mL) was injected into the suspension at room temperature. The solution changed color from light yellow to deep brown and then black ($PtTe_2$) within a few seconds.

Characterization. Scanning electron microscopy (SEM) images were obtained by a JEOL model JSM-6700F. Transmission electron microscopy (TEM) analysis was conducted with a JEOL model JEM-2100F operated at 200 kV. Energy-dispersive X-ray spectrometer (EDX) data were collected using OXFORD INCA x-sight 7421 attached to the JEM-2100F TEM. XRD measurement was performed on a Rigaku II D/MAX X-ray diffractrometer at Cu Kα radiation (λ = 0.1542 nm). The UV−vis absorption spectra were analyzed by a JASCO V-500 UV/vis spectrophotometer. The photoluminescence spectra were obtained with Varian Cary Eclipse at the excitation wavelength of 400 nm.

Acknowledgment. This research was supported by the National Research Foundation (NRF) of Korea funded by the Korea Government (MEST) through WCU program (R32-20031), Pioneer Research Program (008-05103), and Basic Research Support (CIGS(2009-0077998).

Supporting Information Available: SEM and TEM images of various nanowires, nanorods, and nanotubes and EDS analyses of transformed nanowires are displayed. This material is available free of charge *via* the Internet at http://pubs.acs.org.

REFERENCES AND NOTES

1. Mokari, T.; Aharoni, A.; Popov, I.; Banin, U. Diffusion of Gold into InAs Nanocrystals. *Angew. Chem., Int. Ed.* **2006**, *45*, 8001–8005.
2. Yin, Y.; Rioux, R. M.; Erdonmez, C. K.; Hughes, S.; Somorjai, G. A.; Alivisatos, A. P. Formation of Hollow Nanocrystals through the Nanoscale Kirkendall Effect. *Science* **2004**, *304*, 711–714.
3. Schaak, R. E.; Sra, A. K.; Leonard, B. M.; Cable, R. E.; Bauer, J. C.; Han, Y. -F.; Means, J.; Teizer, W.; Vasquez, Y.; Funck, E. X. Metallurgy in a Beaker: Nanoparticle Toolkit for the Rapid Low-Temperature Solution Synthesis of Functional Multimetallic Solid-State Materials. *J. Am. Chem. Soc.* **2005**, *127*, 3506–3515.
4. Robinson, R. D.; Sadtler, B.; Demchenko, D. O.; Erdonmez, C. K.; Wang, L.-W.; Alivisatos, A. P. Spontaneous Superlattice Formation in Nanorods through Partial Cation Exchange. *Science* **2007**, *317*, 355–358.
5. Dloczik, L.; Koenenkamp, P. Nanostructure Transfer in Semiconductors by Ion Exchange. *Nano Lett.* **2003**, *3*, 651–653.
6. Jiang, X. C.; Mayers, B.; Wang, Y. L.; Cattle, B.; Xia, Y. Template-Engaged Synthesis of $RuSe_2$ and $Pd_{17}Se_{15}$ Nanotubes by Reacting Precursor Salts with Selenium Nanowires. *Chem. Phys. Lett.* **2004**, *385*, 472–476.
7. Henkes, A. E.; Schaak, R. E. Trioctylphosphine: A General Phosphorus Source for the Low-Temperature Conversion of Metals into Metal Phosphides. *Chem. Mater.* **2007**, *19*, 4234–4242.
8. Yang, Z.; Smetana, A. B.; Sorensen, C. M.; Kabunde, K. J. Synthesis and Characterization of a New Tiara Pd(II) Thiolate Complex, $[Pd(SC_{12}H_{25})_2]_6$, and Its Solution-Phase Thermolysis To Prepare Nearly Monodisperse Palladium Sulfide Nanoparticles. *Inorg. Chem.* **2007**, *46*, 2427–2431.
9. Cheetham, A. K.; Day, P. *Solid State Chemistry: Techniques*; Clarendon Press: Oxford, 1987.
10. Rao, C. N. R.; Gopalakrishnan, J. *New Directions in Solid State Chemistry*; Cambridge University Press: Cambridge, 1997.
11. Krustok, J.; Madasson, J.; Altosaar, M.; Kukk, P. E. The Nature of Recombination Centres in Silver- and Chlorine-Doped CdS Phosphors. *J. Phys. Chem. Solids* **1990**, *51*, 1013–1018.
12. Lokhande, C. D.; Bhad, V. V.; Dhumure, S. S. Conversion of Tin Disulphide into Silver Sulphide by a Simple Chemical Method. *J. Phys. D: Appl. Phys.* **1992**, *25*, 315–318.
13. Lokhande, C. D.; Gadave, K. M. A Simple Chemical Method for Conversion of CdS into Ag_2S and CdSe into Ag_2Se. *Mater. Chem. Phys.* **1993**, *36*, 119–123.
14. Ristova, M.; Ristov, M. XPS Profile Analysis on CdS Thin Film Modified with Ag by an Ion Exchange. *Appl. Surf. Sci.* **2001**, *181*, 68–77.
15. Son, D. H.; Hughes, S. M.; Yin, Y.; Alivisatos, A. P. Cation Exchange Reactions in Ionic Nanocrystals. *Science* **2004**, *306*, 1009–1012.
16. Camargo, P. H.; Lee, Y. H.; Jeong, U.; Zou, Z.; Xia, Y. Cation Exchange: A Simple and Versatile Route to Inorganic Colloidal Spheres with the Same Size but Different Compositions and Properties. *Langmuir* **2007**, *23*, 2985–2992.
17. Wark, E. S.; Hsia, C. H.; Son, D. H. Effects of Ion Solvation and Volume Change of Reaction on the Equilibrium and Morphology in Cation-Exchange Reaction of Nanocrystals. *J. Am. Chem. Soc.* **2008**, *130*, 9550–9555.
18. Dloczik, L.; Engelhardt, R.; Ernst, K.; Fiechter, S.; Sieber, I.; Könenkamp, R. Hexagonal Nanotubes of ZnS by Chemical Conversion of Monocrystalline ZnO Columns. *Appl. Phys. Lett.* **2001**, *78*, 3687–3689.
19. Jeong, U.; Xia, Y. Large-Scale Synthesis of Single-Crystal Cdse Nanowires through a Cation-Exchange Route. *Chem. Phys. Lett.* **2005**, *416*, 246–250.
20. Jeong, U.; Camargo, P. H. C.; Lee, Y. H.; Xia, Y. Chemical Transformation: A Powerful Route to Metal Chalcogenide Nanowires. *J. Mater. Chem* **2006**, *16*, 3893–3897.
21. Liang, H.-W.; Liu, S.; Wu, Q.-S.; Yu, S.-H. An Efficient Templating Approach for Synthesis of Highly Uniform CdTe and PbTe Nanowires. *Inorg. Chem.* **2009**, *48*, 4927–4933.
22. Liang, H.-W.; Liu, S.; Gong, J.-Y.; Wang, S.-B.; Wang, L.; Yu, S.-H. Ultrathin Te Nanowires: An Excellent Platform for Controlled Synthesis of Ultrathin Platinum and Palladium Nanowires/Nanotubes with Very High Aspect Ratio. *Adv. Mater.* **2009**, *21*, 1850–1854.
23. Xia, Y.; Yang, P.; Sun, Y.; Wu, Y.; Mayers, B.; Gates, B.; Yin, Y.; Kim, F.; Yan, H. One-Dimensional Nanostructures: Synthesis, Characterization, and Applications. *Adv. Mater.* **2003**, *15*, 353–389.
24. Cademartiri, L.; Ozin, G. A. Ultrathin Nanowires—A Materials Chemistry Perspective. *Adv. Mater.* **2009**, *21*, 1013–1020.
25. Cui, Y.; Wei, Q.; Park, H.; Lieber, C. M. Nanowire Nanosensors for Highly Sensitive and Selective Detection of Biological and Chemical Species. *Science* **2001**, *293*, 1289–1292.
26. Nhut, J. M.; Pesant, L.; Tessonnier, J. P.; Wine, G.; Guille, J.; Pham-Huu, C.; Ledoux, M. J. Mesoporous Carbon Nanotubes for Use as Support in Catalysis and As Nanosized Reactors for One-Dimensional Inorganic Material Synthesis. *Appl. Catal., A* **2003**, *254*, 345–363.
27. Hochbaum, A. I.; Chen, R. K.; Delgado, R. D.; Liang, W. J.; Garnett, E. C.; Najarian, M.; Majumdar, A.; Yang, P.

Enhanced Thermoelectric Performance of Rough Silicon Nanowires. *Nature* **2008**, *451*, 163–167.
28. Zhao, X.; Wei, C. M.; Yang, L.; Chou, M. Y. Quantum Confinement and Electronic Properties of Silicon Nanowires. *Phys. Rev. Lett.* **2004**, *92*, 1–4.
29. Pascual, J. I.; Mendez, J.; Gomezherrero, J.; Baro, A. M.; Garcia, N.; Landman, U.; Luedtke, W. D.; Bogachek, E. N.; Cheng, H. P. Properties of Metallic Nanowires: From Conductance Quantization to Localization. *Science* **1995**, *267*, 1793–1795.
30. Seo, K.; Varadwaj, K. S. K.; Mohanty, P.; Lee, S.; Jo, Y.; Jung, M. H.; Kim, J.; Kim, B. Magnetic Properties of Single-Crystalline CoSi Nanowires. *Nano Lett.* **2007**, *7*, 1240–1245.
31. Dresselhaus, M. S.; Chen, G.; Tang, M. Y.; Yang, R.; Lee, H.; Wang, D.; Ren, Z.; Fleurial, J. P.; Gogna, P. New Directions for Low-Dimensional Thermoelectric Materials. *Adv. Mater.* **2007**, *19*, 1043–1053.
32. Hong, B. H.; Bae, S. C.; Lee, C. W.; Jeong, S.; Kim, K. S. Ultrathin Single-Crystalline Silver Nanowire Arrays Formed in an Ambient Solution Phase. *Science* **2001**, *294*, 348–351.
33. Coleman, N. R. B.; Morris, M. A.; Spalding, T. R.; Holmes, J. D. The Formation of Dimensionally Ordered Silicon Nanowires within Mesoporous Silica. *J. Am. Chem. Soc.* **2001**, *123*, 187–188.
34. Peng, X. G.; Manna, L.; Yang, W. D.; Wickham, J.; Scher, E.; Kadavanich, A.; Alivisatos, A. P. Shape Control of CdSe Nanocrystals. *Nature* **2000**, *404*, 59–61.
35. Liu, Z. P.; Xu, D.; Liang, J. B.; Shen, J. M.; Zhang, S. Y.; Qian, Y. T. Growth of Cu_2S Ultrathin Nanowires in a Binary Surfactant Solvent. *J. Phys. Chem. B* **2005**, *109*, 10699–10704.
36. Banfield, J. F.; Welch, S. A.; Zhang, H. Z.; Ebert, T. T.; Penn, R. L. Aggregation-Based Crystal Growth and Microstructure Development in Natural Iron Oxyhydroxide Biomineralization Products. *Science* **2000**, *289*, 751–754.
37. Colfen, H.; Antonietti, M. Mesocrystals: Inorganic Superstructures Made by Highly Parallel Crystallization and Controlled Alignment. *Angew. Chem., Int. Ed.* **2005**, *44*, 5576–5591.
38. Tsuruoka, T.; Furukawa, S.; Takashima, Y.; Yoshida, K.; Isoda, S.; Kitagawa, S. Nanoporous Nanorods Fabricated by Coordination Modulation and Oriented Attachment Growth. *Angew. Chem., Int. Ed.* **2009**, *48*, 4739–4743.
39. Mayers, B. T.; Gates, B.; Xia, Y. One-Dimensional Nanostructures of Chalcogens and Chalcogenides. *Int. J. Nanotechnol.* **2004**, *1*, 86–104.
40. Qian, H.-S.; Yu, S.-H.; Gong, J.-Y.; Luo, L.-B.; Fei, L.-f. High-Quality Luminescent Tellurium Nanowires of Several Nanometers in Diameter and High Aspect Ratio Synthesized by a Poly(vinyl pyrrolidone): Assisted Hydrothermal Process. *Langmuir* **2006**, *22*, 3830–3835.
41. Lin, J.-H.; Yan, J.; Chang, H.-T. Preparation of Fluorescent Tellurium Nanowires at Room Temperature. *Cryst. Growth Des.* **2008**, *8*, 351–357.
42. Lu, Q.; Gao, F.; Komarneni, S. Biomolecule-Assisted Reduction in the Synthesis of Single-Crystalline Tellurium Nanowires. *Adv. Mater.* **2004**, *16*, 1629–1632.
43. Mo, M.; Zeng, J.; Liu, X.; Yu, W.; Zhang, S.; Qian, Y. Controlled Hydrothermal Synthesis of Thin Single-Crystal Tellurium Nanobelts and Nanotubes. *Adv. Mater.* **2002**, *14*, 1658–1662.
44. Liu, Z.; Hu, Z.; Liang, J.; Li, S.; Yang, Y.; Peng, S.; Qian, Y. Size-Controlled Synthesis and Growth Mechanism of Monodisperse Tellurium Nanorods by a Surfactant-Assisted Method. *Langmuir* **2004**, *20*, 214–218.
45. Cotton, F. A.; Wilkinson, G.; Murillo, C. A.; Bochmann, M. *Advanced Inorganic Chemistry*, 6th ed.; Wiley-Interscience: New York, 1999.
46. Jeong, U.; Xia, Y. Photonic Crystals with Thermally Switchable Stop Bands Fabricated from Se@Ag_2Se Spherical Colloids. *Angew. Chem., Int. Ed.* **2005**, *44*, 3099–3103.
47. Gates, B; Mayers, B; Wu, Y.; Sun, Y.; Cattle, B; Yang, P.; Xia, Y. Synthesis and Characterization of Crystalline Ag_2Se Nanowires through a Template-Engaged Reaction at Room Temperature. *Adv. Funct. Mater.* **2002**, *12*, 679–686.
48. Mu, L.; Wan, J.; Zhang, R.; Yu, W.; Qian, Y. A Room Temperature Self-Sacrificing Template Route to Ag_2Te Fibers. *Chem. Lett.* **2005**, *34*, 52–53.
49. Mayers, B.; Jiang, X. C.; Sunderland, D.; Cattle, B.; Xia, Y. Hollow Nanostructures of Platinum with Controllable Dimensions Can Be Synthesized by Templating Against Selenium Nanowires and Colloids. *J. Am. Chem. Soc.* **2003**, *125*, 13364–13365.
50. Frueh, A. J. The Structure of Hessite, Ag_2Te. *Z. Kristallogr.* **1959**, *112*, 44–52.
51. Hefter, G. T.; Tomkins, R. P. T. *The Experimental Determination of Solubilities*; John Wiley and Sons, Ltd.: NewYork, 2003.
52. kolthoff, I. M. The Solubilities and Solubility Products of Metallic Sulphides in Water. *J. Phys. Chem.* **1931**, *35*, 2711–2721.
53. Hodes, G. *Chemical Solution Deposition of Semiconductor Films*; Marcel Dekker, Inc.: New York, 2003.
54. Lide, D. R *CRC Handbook of Chemistry and Physics*; CRC-Press: Boca Raton, FL, 2009.
55. Lubeck, C. R.; Han, T. Y. J.; Gash, A. E.; Satcher, J. H., Jr.; Doyle, F. M. Synthesis of Mesostructured Copper Sulfide by Cation Exchange and Liquid-Crystal Templating. *Adv. Mater.* **2006**, *18*, 781–784.
56. Grebinski, J. W.; Hull, K. L.; Zhang, J.; Kosel, T. H.; Kuno, M. Solution-Based Straight and Branched CdSe Nanowires. *Chem. Mater.* **2004**, *16*, 5260–5272.
57. Baleva, M.; Mateeva, E. Pressure Coefficient of the PbTe Metastable CsCl-Type-Phase Energy Gap. *Phys. Rev. B* **1994**, *50*, 8893–8896.
58. Dziawa, P.; Sadowski, J.; Dluzewski, P.; Lusakowska, E.; Domukhovski, V.; Taliashvili, B.; Wojciechowski, T.; Baczewski, L. T.; Bukala, M.; Galicka, M.; *et al.* Defect Free PbTe Nanowires Grown by Molecular Beam Epitaxy on GaAs(111)B SubstratesM. *Cryst. Growth Des.* **2010**, *10*, 109–113.
59. Fedorov, V. A.; Ganshin, Y. N.; Korkishko, Y. N. Determination of the Point of the Zincblende-to-Wurtzite Structural Phase Transition in Cadmium Selenide Crystals. *Phys. Status Solidi A* **1991**, *126*, K5–K7.
60. Yeh, C.-Y.; Lu, Z. W.; Froyen, S.; Zunger, A. Zinc-Blende-Wurtzite Polytypism in Semiconductors. *Phys. Rev. B* **1992**, *46*, 10086–10097.
61. Isomaki, H. M.; Boehm, J. V. Optical Absorption of Tellurium. *Phys. Scr.* **1982**, *25*, 801–803.
62. Gautam, U. K.; Rao, C. N. R. Controlled Synthesis of Crystalline Tellurium Nanorods, Nanowires, Nanobelts and Related Structures by a Self-Seeding Solution Process. *J. Mater. Chem.* **2004**, *14*, 2530–2535.